

Deep Koopman-operator based model predictive control for closed-loop electrical neurostimulation in epilepsy

Zhichao Liang[†], Zixiang Luo[†], Keyin Liu, Jingwei Qiu and Quanying Liu^{*}

Abstract—**Electrical neuromodulation as a palliative treatment has been increasingly applied to epilepsy. However, most of the current neuromodulation implement pre-determined actuation strategies rather than closed-loop neurofeedback. In this paper, rooted in optimal control theory, we propose a novel framework for real-time closed-loop electrical neuromodulation in epilepsy. Our framework combines a deep Koopman-operator based model for seizure prediction in an approximated finite dimensional linear dynamics and the model predictive control (MPC) for designing optimal seizure suppression strategies. We validate our model with synthetic seizure data from Jansen-Rit Model which generates neural dynamics in a single cortical column and two distant cortical columns. The results demonstrate that the deep Koopman-operator based model has great capabilities to map the nonlinear neural dynamics into finite dimensional linear dynamics, which is suitable for real-time seizure prediction and naturally compatible with the optimal-based linear MPC design for seizure suppression. Our framework opens a new window for the development and implementation of robust real-time closed-loop electrical neuromodulation in epileptic seizure suppression and sheds light on understanding the neurodynamics and feedback control policies.**

I. INTRODUCTION

Epilepsy is a neurological disorder characterized by the occurrence of a spontaneous seizure, a period when neuron population fires in an abnormal, excessive, and synchronized manner [1], [2]. In clinical, the main characteristics for diagnosis of epilepsy are occurring the seizure-like spike-and-wave and high-frequency oscillations [3]. Electroencephalogram (EEG), stereo electroencephalogram (sEEG), and intracranial electroencephalogram (iEEG) are the main techniques for monitoring seizures [4].

Recently, various therapies have been developed for treating and controlling seizures, including anti-epilepsy medication, surgical extraction, and electrical neurostimulation [5]. Electrical neurostimulation, such as deep brain stimulation (DBS) and transcranial electrical stimulation (TES), has become a considerable clinical treatment for intractable epilepsy. Electrical neurostimulation applies a minuscule dose of high-frequency electric current to a brain region, such as a cortex area, vagus nerve, or anterior nucleus of thalamus. This electrical stimulation aims to modulating the neural oscillations and thus controlling the seizure states.

This work was supported by National Natural Science Foundation of China (No. 62001205), Guangdong Natural Science Foundation Joint Fund (No. 2019A1515111038).

Z. Liang, Z. Luo, K. Liu, J. Qiu and Q. Liu are with Department of Biomedical Engineering, Southern University of Science and Technology, Shenzhen, China.

[†] Co-first authors: Zhichao Liang, Zixiang Luo

^{*} Corresponding author: Quanying Liu liuqy@sustech.edu.cn

However, the current neuromodulations mainly implement the pre-determined actuation strategies rather than a closed-loop electrical neurostimulation in epilepsy. Traditional deep brain stimulation and neurostimulator paradigms are designed with empirical open-loop approaches, lacking of theoretical supports or guarantees. A major disadvantage of open-loop neurostimulation is missing the feedback signals of current seizure waves to regulate the control input during neurostimulation. More recently, closed-loop mechanisms is increasingly gaining attention for seizure suppression. Formatting it as a closed-loop state-space control problem, the main goal then is to design an optimal control law to steer the system state to the desired state. Some previous work have been devoted to this area. For example, Sérgio Pequito et al. presented a spectral control method for ensuring the poles of the closed-loop systems in the pre-specified spectrum [6]. Arian Ashourvan et al. proposed a pole-placement spectral static output feedback control-theoretic strategy for linear time-invariant switching systems for seizure stabilizing [7]. Model predictive control (MPC) is a self-tuning control method, allowing to maintain a stable and robust control process, which has been brought into neurostimulation applications. For instance, Siyuan Chang et al. presented a nonlinear auto-regressive moving-average (NARMA) Volterra model to identify the relationship between the external input and the corresponding neuronal responses such as synthetic seizure-like waves, based on which the closed-loop MPC actuation strategy was implemented to optimize the stimulator's waveform [8]. Sarthak Chatterjee et al. proposed a fractional-order model predictive control framework for real-time closed-loop electrical neurostimulation in epilepsy [9]. However, the MPC requires a decent model to predict the system dynamics, which is particularly challenging for seizure dynamics.

Seizure dynamics is a complex networked nonlinear dynamic process, and we have limited knowledge on the dynamics of seizure so far. Therefore, system identification is crucial for uncovering the brain system dynamics during seizure period. Some tools are available for modeling the seizure system dynamics using time-series EEG data. For example, auto-regressive moving-average model [8] and fractional-order system model [9] have been applied for seizure dynamics identification. With the advances of machine learning methods, data-driven models have shown great potentials as a system identification tool. For example, recurrent neural network (RNN) is promising in fitting time-series data and modeling dynamical systems. Some studies have reported that RNN has high capability and scalability

in modeling complex dynamics with multi-outputs, such as fluidic flow control [10] and process industries [11]. However, most of RNN models are time consuming and hardly integrated into MPC to solve the optimization problem.

It is necessary to consider the trade-off between model complexity and computational efficiency when modeling seizure dynamics and designing controller for seizure suppression. The real-time optimal solution of a nonlinear complex dynamics model in MPC is hard to obtain. To address this issue, operator-theoretic approaches, mainly based on the Perron-Frobenius operator [12] or its adjoint Koopman-operator, are increasingly gaining attention. In particular, Koopman theory states that nonlinear dynamics of a system can be linearized under the hypothesis that the linear operator acts on the observation function of system states with advancing in time [13]. However, a pre-defined hand-crafted Koopman-operator model has limited performance in modeling time-varying or complex switching dynamical systems. Therefore, a more flexible way to approximate the Koopman-operator with finite dimensions is needed. Recently, some autoencoder-based methods for approximating finite-dimensional Koopman-operator was proposed [14], [15]. After Koopman-operator converts a nonlinear MPC problem to a linear MPC problem, it can be easily solved by a quadratic programming solver.

Here, we propose a deep Koopman-operator based model predictive control (Koopman-MPC) framework for closed-loop seizure suppression in a real-time manner, which can balance the needs of sufficient predictive accuracy and model complexity for the real-time optimization. The contributions of this study are summarized as follows.

- Koopman-MPC framework maps the nonlinear neural dynamics into finite-dimensional linear dynamics using a deep Koopman-operator based model, which is computationally efficient and naturally compatible with the optimization-based MPC design for seizure suppression.
- A tailored autoencoder model is designed to approximate the Koopman-operator with finite dimensions, which avoids hand-crafted design of Koopman-operator. Our results suggest that the deep Koopman model outperforms the RNN model in seizure prediction.
- We experimentally verify the Koopman-MPC framework with a simulation platform based on Jansen-Rit model, confirming that Koopman-MPC suppress seizures from one region as well as seizures propagated between brain regions.

II. METHOD

A. Koopman-operator

Given a discrete-time dynamical system

$$\mathbf{x}_{k+1} = \mathbf{f}(\mathbf{x}_k), \quad (1)$$

where \mathbf{x}_k denotes the vector of state variables and \mathbf{f} governs the system dynamics. Koopman operator \mathbf{K} is defined as a linear operator acting on an infinite dimensional function space such that for any observation function g ,

$$\mathbf{K}g(\mathbf{x}) = g(\mathbf{f}(\mathbf{x})). \quad (2)$$

The key idea of the Koopman-operator is to design a nonlinear embedding transformation into a linear dynamical system. The embedding transformation can be obtained by a finite-dimensional approximation of the Koopman-operator, in which an invariant subspace or a set of basis functions is determined or learned. Extended Dynamic Mode Decomposition is a data-driven method commonly used for numerical approximation of the Koopman-operator, and it allows arbitrary composition of basis functions for dynamics approximation[16].

Given a finite sequence of system measurements $\mathbf{y}_i = \mathbf{g}(\mathbf{x}_i)$ and a finite set of basis functions $\Phi_1, \Phi_2, \dots, \Phi_k$ constituting a basis function vector $\Phi = [\Phi_1, \Phi_2, \dots, \Phi_k]^T$, we can embed the data into the basis function vector and construct two feature spaces,

$$\begin{aligned} \Psi_Y &= [\Phi(\mathbf{y}_1) \quad \Phi(\mathbf{y}_2) \quad \dots \quad \Phi(\mathbf{y}_k)] \\ \Psi_{\tilde{Y}} &= [\Phi(\tilde{\mathbf{y}}_1) \quad \Phi(\tilde{\mathbf{y}}_2) \quad \dots \quad \Phi(\tilde{\mathbf{y}}_k)] \end{aligned} \quad (3)$$

where $\tilde{\mathbf{y}}_k = \mathbf{y}_{k+1}$. Then the finite-dimensional approximation of the Koopman-operator $\tilde{\mathbf{K}}$ can be inferred from

$$\tilde{\mathbf{K}} = \Psi_{\tilde{Y}} \Psi_Y^\dagger \quad (4)$$

where Ψ_Y^\dagger is the pseudo-inverse of Ψ_Y .

Modal decomposition for Koopman-operator \mathbf{K} refers to spectral analysis [17], in which its modes and eigenvalues-eigenvector pairs characterize the complex linear independent spatiotemporal dynamical behaviours. The complex eigenvalues of \mathbf{K} characterize the system stability, exponential damping ratio and spectral information, and the eigenvectors represent the independent spatial coordinates. This linear operator \mathbf{K} can be used for the prediction and control of system dynamics.

B. Koopman-operator based model predictive control

Model predictive control is an optimization-based control framework to minimize the control objective function in a finite prediction horizon with the control inputs and states constraints. For a nonlinear dynamical system, the optimization problem is typically a non-convex problem with NP-hard computational complexity.

The predictive capabilities and linearity of the Koopman-operator benefit the controller design in nonlinear systems. Therefore, we construct a Koopman-operator based model predictive control architecture to control the nonlinear system following the desired reference signals, as shown in Fig. 1(a).

At each time-step, the model predictive control solves the following objective function to find a sequence of incremental inputs Δu_k and only the first incremental input Δu_1 will be applied to the system.

$$\begin{aligned} \min_u \quad & \left\{ \sum_{k=1}^{T_p} (\mathbf{Y}_k - \mathbf{Y}_{\text{ref}})^T \mathbf{Q}_Y (\mathbf{Y}_k - \mathbf{Y}_{\text{ref}}) + \mathbf{Q}_u \sum_{k=1}^{T_c} \Delta u_k^2 \right\} \\ \text{s.t.} \quad & \Delta u_k \in [\Delta u_{\min}, \Delta u_{\max}] \\ & u_k \in [u_{\min}, u_{\max}] \\ & \mathbf{Y}_{k+1} = \tilde{\mathbf{K}} \mathbf{Y}_k + \mathbf{B} u_k \end{aligned} \quad (5)$$

where T_p and T_c are the predictive horizon and control horizon, respectively. \mathbf{Y}_k and \mathbf{Y}_{ref} represent the Koopman

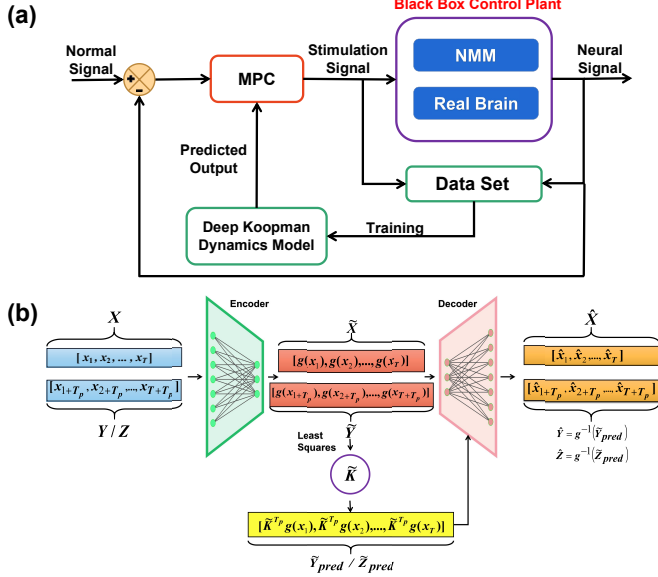


Fig. 1. Schematic of the deep Koopman-operator based model predictive control for dynamics identification and closed-loop electrical neurostimulation in epilepsy. (a) An MPC framework for epileptic seizure suppression. (b) The autoencoder-based deep Koopman dynamical model. Y and Z are used for one-step and multi-step prediction. T_p equals 1 and 20 for Y and Z , respectively.

basis function of the observation and reference signals, respectively. Δu_k is the increment of input at step k . \mathbf{Q}_Y is the positive definite weighted matrix for penalizing the deviance and \mathbf{Q}_u is a non-negative scalar to penalize the amplitudes of control incremental inputs and tune the desired closed-loop control performance. For real applications, the inputs are constrained between the upper bound and lower bound. $\mathbf{Y}_{k+1} = \tilde{\mathbf{K}}\mathbf{Y}_k + \mathbf{B}\Delta u_k$ predicts the following states in the predictive horizon. $\tilde{\mathbf{K}}$ is the approximated unforced Koopman-operator when there are no inputs or the forced Koopman-operator when giving input signals [14]. \mathbf{B} is designed by the researcher to determine the control gain in corresponding latent controlled nodes. This optimization problem can be solved efficiently with the Quadratic Programming Solver. In this case, the input signal is constrained between -25 to 0 and the increment of it is constrained between -20 to 0. \mathbf{Q}_Y is set to an identity matrix. \mathbf{Q}_u equals 0.01.

III. DEEP KOOPMAN-OPERATOR MODEL

For learning the finite-dimensional invariant subspace to approximate the Koopman-operator, we construct an autoencoder framework, similar to the previous work [14], [15], but different model hidden structure and loss function, to span a low dimensional state space of the observed seizure dynamics into a finite high dimensional state space. The deep Koopman-operator model is shown in Fig.1(b). Specifically, the encoder learns the linear mapping relationship (a finite-dimensional approximated Koopman-operator) between one prior step and the current step of the sequential seizure waves. Then, we decode the spanning data and its predicted data into the original state space for reconstruction.

A. Seizure Dynamic Encoder in an Autoencoder Architecture

Both the encoder and decoder contain one hidden dense layer followed by a rectified linear unit activation and an output dense layer. The inputs to the encoder are pieces of epilepsy signals X , Y , and Z that constructed with a sequence of time snapshots. The encoder produces the high dimensional matrices \tilde{X} , \tilde{Y} , and \tilde{Z} . Then, the the Koopman-operator $\tilde{\mathbf{K}}$ was approximated by a linear least-squares fit between \tilde{X} and \tilde{Y} . Using the Koopman operator, \tilde{Y}_{pred} and \tilde{Z}_{pred} are computed as $\tilde{\mathbf{K}}\tilde{X}$ and $\tilde{\mathbf{K}}^{T_p}\tilde{X}$. Finally, the \hat{X} , \hat{Y} , and \hat{Z} are the decoded signals from \tilde{X} , \tilde{Y}_{pred} , and \tilde{Z}_{pred} . More details are shown in Appendix B.1.

B. Explicit Loss Definition

The deep Koopman-operator based autoencoder model is trained to minimize the following four reconstruction error terms (Mean-squared error, MSE). The loss is specifically designed with different theoretical considerations for learning the finite-dimensional approximated Koopman-operator and building the linear dynamical system. The defined MSE terms include a Reconstruction Loss (\mathcal{L}_{recon}), a Prediction Loss of Y ($\mathcal{L}_{Y_{pred}}$), a T_p -step Prediction Loss of Z ($\mathcal{L}_{Z_{pred}}$), and a Linear Dynamics Reconstruction Loss (\mathcal{L}_{lin}). Meanwhile, a \mathcal{L}_2 regularization term is added to the weights \mathbf{W} to avoid overfitting.

$$\mathcal{L} = \mathcal{L}_{recon} + \mathcal{L}_{Y_{pred}} + \mathcal{L}_{Z_{pred}} + \mathcal{L}_{lin} + \alpha \|\mathbf{W}\|_2^2 \quad (6)$$

$$\mathcal{L}_{recon} = \|\mathbf{X} - g^{-1}(\mathbf{g}(\mathbf{X}))\|_2^2 = \|\mathbf{X} - \hat{\mathbf{X}}\|_2^2 \quad (7)$$

$$\mathcal{L}_{Y_{pred}} = \|\tilde{\mathbf{Y}}_{pred} - g^{-1}(\tilde{\mathbf{K}}\mathbf{g}(\mathbf{X}))\|_2^2 = \|\tilde{\mathbf{Y}}_{pred} - \hat{\mathbf{Y}}\|_2^2 \quad (8)$$

$$\mathcal{L}_{Z_{pred}} = \|\tilde{\mathbf{Z}}_{pred} - g^{-1}(\tilde{\mathbf{K}}^{T_p}\mathbf{g}(\mathbf{X}))\|_2^2 = \|\tilde{\mathbf{Z}}_{pred} - \hat{\mathbf{Z}}\|_2^2 \quad (9)$$

$$\mathcal{L}_{lin} = \|\mathbf{g}(\mathbf{Y}) - \tilde{\mathbf{K}}\mathbf{g}(\mathbf{X})\|_2^2 = \|\tilde{\mathbf{Y}} - \tilde{\mathbf{K}}\tilde{\mathbf{X}}\|_2^2 \quad (10)$$

The matrix $\tilde{\mathbf{K}}$ represents the approximated Koopman-operator. T_p represents the predictive length. g and g^{-1} are the encoder and decoder expression, respectively. We set the hyperparameter $\alpha = 0.01$ by default.

To sum up, our proposed Deep Koopman-operator model learns the invariant linear subspace of seizure dynamics for further seizure prediction and seizure stimulation strategy design.

IV. EXPERIMENTS

A. Datasets

We validate the deep Koopman-operator based MPC model for seizure suppression using synthetic data from a single cortical column and two distant cortical columns. All synthetic EEG data are generated by a well-known computational dynamical model, *i.e.* the Jansen-Rit model [18].

In the past two decades, dynamical models have become a popular method to model neurological disorders (*e.g.* epilepsy) from the microscopic level [19] to the macroscopic level [20], [21]. The neural mass model (NMM) simulates the neural signals from a cortical column at the macroscopic

level, with excitatory population, inhibitory populations and pyramidal cells interaction [18]. As a specific neural mass model, the Jansen-Rit model uses six dynamical equations to describe a cortical column's average neural activities, including a population of pyramidal cells, the excitatory feedback interneurons and the inhibitory feedback interneurons [18]. The Jansen-Rit model is given by the following dynamical system.

$$\begin{cases} \dot{y}_1 = y_4 \\ \dot{y}_4 = AaS(y_2 - y_3) - 2ay_4 - a^2y_1 \\ \dot{y}_2 = y_5 + d(t) \\ \dot{y}_5 = Aa(p + C_2S(C_1y_1)) - 2ay_5 - a^2y_2 \\ \dot{y}_3 = y_6 \\ \dot{y}_6 = BbC_4S(C_3y_1) - 2by_6 - b^2y_3 \end{cases} \quad (11)$$

The detailed information about the Jansen-Rit model is shown in the Appendix A. The parameters setting for Jansen-Rit NMM is shown in Table S1. These values were originally specified by Van Rotterdam et al. [22]. In our simulation, we keep the above parameters fixed and vary the excitatory synaptic gain A (*i.e.*, a bifurcation parameter). The model generates normal state EEG waves when A equals 7, and it generates seizure-like waves with A larger than the critical value (around 7.2115). We display three types of synthetic EEG signal with different excitatory synaptic gain ($A \in \{7.0, 7.2115, 7.80\}$) in Fig. 2(a-c). For simulation, we collect the input and the output data with a 50 Hz sampling rate.

To investigate whether the model can predict the data from multiple neural sites, we also simulated the seizure data from two interactive cortical columns using the Jansen-Rit Model. The detailed information about using the Jansen-Rit model to generate EEG data in the double cortical columns is shown in the Appendix A. One of the cortical columns ($A = 7.8$) generates the seizure-like wave and propagates to another non-seizure cortical column ($A = 7.0$); the non-seizure cortical column, therefore, forms the induced seizure-like waves. Fig. 3(a) illustrates the simulated data from two cortical columns.

B. Deep Koopman-operator based seizure prediction

We conducted experiments to test the capability of the Deep Koopman-operator model in seizure prediction in two cases: 1) the seizure-like wave is focused on a single cortical column; 2) the seizure waves propagate to two cortical columns. To evaluate the prediction accuracy of our deep Koopman-operator model on validation datasets, we introduce two quantitative metrics: the Mean-Squared-Error (MSE) and the R-Square (R^2).

$$\begin{aligned} \text{MSE} &= \frac{1}{T_{\text{pred}}} \sum_{k=1}^{T_{\text{pred}}} \|y_k - \hat{y}_k\|_2^2 \\ R^2 &= 1 - \frac{\sum_{k=1}^{T_{\text{pred}}} (\hat{y}_k - y_k)^2}{\sum_{k=1}^{T_{\text{pred}}} (y_k - \bar{y})^2} \end{aligned} \quad (12)$$

where y_k is the ground truth, \hat{y}_k is the predictive results, and \bar{y} is the mean value of the ground truth. T_{pred} is the predictive length.

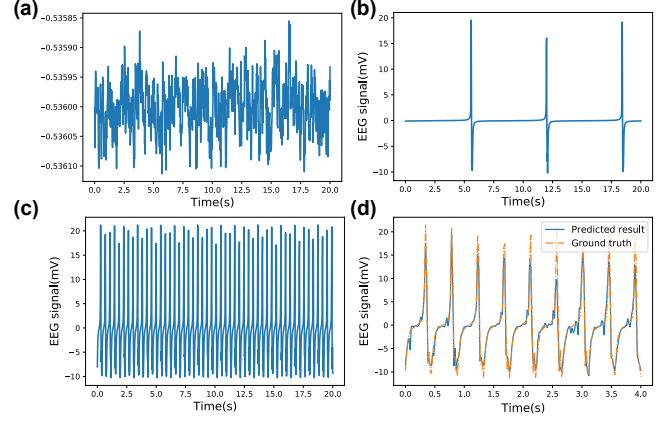


Fig. 2. The synthetic EEG waves from the Jansen-Rit model with a single cortical column. Specifically, (a) $A = 7.0$ corresponds to the normal EEG state; (b) $A = 7.2115$ represents the transition state where the seizure emerges; (c) 7.80 are epileptic states; (d) the predicted seizure-like EEG wave in single cortical column using the deep Koopman-operator method. The excitatory synaptic gain is $A = 7.80$. The Koopman-operator is updated every 20 steps.

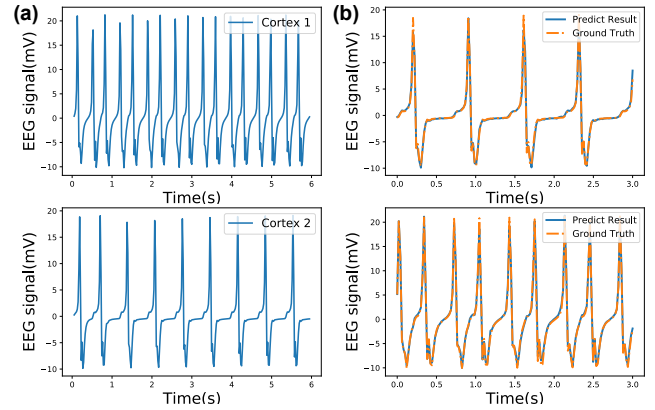


Fig. 3. Seizure-like EEG waves in two cortical columns: (a) the simulated seizure-like EEG waves using the Jansen-Rit model; (b) the predicted EEG dynamics using the deep Koopman-operator method. The excitatory synaptic gain $A = 7.80$ in Cortical 1 (upper) and $A = 7.00$ in Cortical 2 (bottom). The Koopman-operator is updated every 20 steps.

The deep Koopman-operator based model maps the states to an invariant subspace and derived the approximated Koopman-operator \tilde{K} in this invariant subspace. The results of the predictive evaluation from Koopman model are shown in Fig. 2(d) and Fig. 3(b). It indicates that the Koopman-operator based model can successfully predict EEG and seizure waves.

Furthermore, we compare our Koopman model with another data-driven predictive model, *i.e.* Gated Recurrent Units (GRU) model. As a variant of Long Short-Term Memory (LSTM), GRU is rooted in the RNN structure [23]. Here, an additional Dense layer in GRU is trained for capturing the mapping relationship between the previous input/output signals and the initial states of GRU (with 60 hidden units). Also, another Dense layer is trained for mapping the GRU states to the output signals. More details of GRU setting are in Appendix B.2. The performance of GRU model is

TABLE I
MODEL COMPARISONS FOR SEIZURE PREDICTION

Case	Model	MSE	R^2
Single column	GRU	6.2555	0.8502
	Koopman	3.8187	0.8851
Double columns	GRU	5.0832	0.8589
	Koopman	0.5269	0.9866

shown in Appendix Fig.8. The quantitative comparisons of results are shown in TABLE I, suggesting that our deep Koopman-operator based model outperforms the GRU model in both cases. As a highly nonlinear model, GRU might need more hidden units to fit the dynamics of the signal. More interestingly, both the Koopman and GRU model better predicts the data from two cortical columns than from single column, inferring that more interactive information provided would benefit the training of deep Koopman-operator model.

C. MPC-based Seizure Suppression

Generally, the Koopman-operator based predictive model hardly tracks the seizure dynamics for a long period. Therefore, our proposed Koopman-MPC model is designed to periodically re-calculate the approximated Koopman-operator, estimate the corresponding predictions, and then re-compute the optimal neurostimulation strategy.

We conducted experiments to test the Koopman-MPC performance of seizure suppression in two cases. Specifically, we collect the input and output data with a 50Hz sampling frequency. We use a 15-step predictive horizon and 15-step control horizon to calculate the optimal seizure stimulation signals.

Fig.4 illustrates the suppressed seizure in EEG signals and the corresponding control signal designed by the Koopman-MPC controller. In each experiment, the control signal starts to insert into the model at $t = 4s$. It is obvious that the actuation signals is also activated at the 4s during the simulation. These results demonstrate that our Koopman-MPC can accurately predict the seizure signal and achieve a successful seizure suppression.

We then try to compare the control performance from Koopman-MPC and GRU-MPC framework. The objective function in the GRU-MPC framework becomes an NP-hard non-convex optimization problem for the trained GRU is a complex nonlinear model. In our experiment, the GRU-MPC failed to converge to the optimal value. Therefore, we could not compare the seizure suppression results from the non-convex GRU-MPC controller and convex Koopman-MPC controller.

V. DISCUSSION

Here we propose a novel deep Koopman-MPC framework for closed-loop electrical neurostimulation. A tailored autoencoder was employed to learn the invariant subspace of the Koopman-operator, in which a coordinate transformation maps the nonlinear dynamics into the linear dynamics. The approximation of the Koopman-operator provides a sufficient

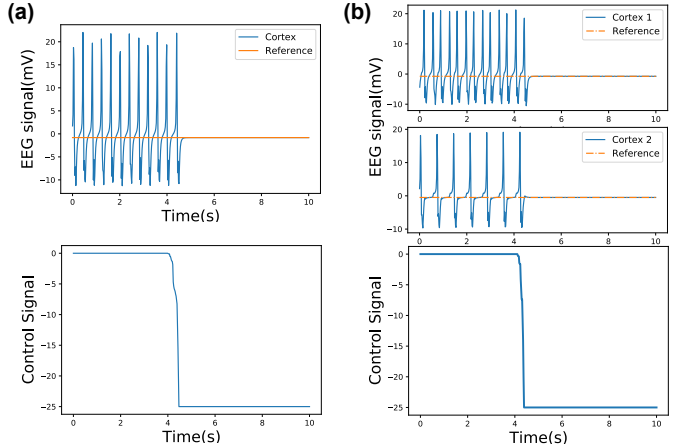


Fig. 4. The seizure suppression and control signal from the Koopman-MPC based closed-loop neurostimulation. The control starts at 4s.(a) The single cortical column case; (b) The double cortical column case. Control input is exerted to the first column.

prediction horizon in seizure prediction, which can be integrated into the MPC controller for seizure suppression. Notably, although the Koopman-MPC framework is motivated by neurostimulation strategy in seizure suppression, it is of broader interest and suitable for other feedback control applications, such as flow control.

1) *Prediction and Control for Seizure Dynamics:* The dynamical system of seizure is a black-box. System identification techniques is beneficial for the prediction and modeling of seizure dynamics and contribute to optimizing neurostimulation strategy in the model-based seizure suppression. However, uncovering the system dynamics has to consider both the accuracy and the model complexity. The latter property is particularly important when it combines with a MPC to solve a optimization problem in real-time. In this study, we made a quantitative comparison of prediction accuracy between our proposed Koopman model and the GRU model with the same number of hidden units. The results suggest that our proposed Koopman model outperforms the GRU model in terms of prediction performance (Table I). One possible reason is that deep Koopman model learns its invariant subspace and captures sufficient nonlinear patterns in its hidden layers for seizure prediction. More important, another favorable merit of the Koopman model is its linear property which greatly facilitates the optimization in MPC control and provides a unique optimal solution. In contrast, the GRU-MPC model failed to converge and could not achieve an optimal control policy in our experiments. In fact, it is most likely a trade-off between model complexity and computational efficiency when designing model for real-time control. A higher-order complex model might better identify the system, but it is computationally expensive in optimization. Along this line, a significant advantage of Koopman-MPC model is that it uses a finite dimension approximated Koopman-operator model for linear optimal control, and balances the accuracy (Table I) and computationally efficiency in convex optimization (Fig. 4). However,

the brain is a complex coupled network dynamic system. Balancing speed and accuracy in the computational model of brain network is one of the challenges in the field of control theory, and it will further drive the development of control theory. For instance, controlling the complex network in brain calls for layered dynamical network models and network control theory. In return, the development of control theory would provide new tools for neurostimulation, including the selection of the optimal targeted stimulation regions, the optimal and robust stimulation protocols.

2) *Limitations and future works:* It is worthy to mention the limitations of our work. First, due to ethical reasons, it is almost impossible to collect input-output data from epilepsy patients as a biological experiment. Thus, we used the Jansen-Rit model to simulate the EEG data and ran MPC experiments based on this simulation platform. The Jansen-Rit model seems to generate seizure-like waves with a fixed pattern (Fig. 2), which is far away from a real case. Other computational dynamical models have been proposed as neural data generators [24], [25]. Developing a reliable simulation platform to generate the seizure-like waves with the preictal, ictal and postictal processes, is an important future direction. Second, our proposed deep Koopman-operator based model allows to predict seizure wave, but it cannot identify the probability of seizure occurrence. Integrating a probabilistic seizure prediction and classification model into our model might improve neurostimulation outcome. Moreover, the decomposition of Koopman-operator could reflect the spectral information about the system dynamics [17], which can be applied to investigate the spectral properties of EEG and seizure dynamics in the future. Our next goal is to improve the interpretability of deep Koopman-operator model. To this end, it is necessary to consider the physical intuitions and neuroscience insights from asymptotic theory and spectral information perspective when designing the model structure, the dimension of the embedding space, the objective function and constraints [26].

VI. ACKNOWLEDGMENTS

The authors gratefully acknowledge Dr. Yi Yao and Prof. Haiyan Wu for the useful discussions, as well as the reviewers' comments.

Authors declare to have no conflict of interests.

REFERENCES

- [1] R. S. Fisher, C. Acevedo, A. Arzimanoglou, A. Bogacz, J. H. Cross, C. E. Elger, J. Engel Jr, L. Forsgren, J. A. French, M. Glynn *et al.*, “Iiae official report: a practical clinical definition of epilepsy,” *Epilepsia*, vol. 55, no. 4, pp. 475–482, 2014.
- [2] J. Yuan, X. Ran, K. Liu, C. Yao, Y. Yao, H. Wu, and Q. Liu, “Machine learning applications on neuroimaging for diagnosis and prognosis of epilepsy: A review,” *arXiv preprint arXiv:2102.03336*, 2021.
- [3] P. Perucca, F. Dubeau, and J. Gotman, “Intracranial electroencephalographic seizure-onset patterns: effect of underlying pathology,” *Brain*, vol. 137, no. 1, pp. 183–196, 2014.
- [4] P. Jayakar, J. Gotman, A. S. Harvey, A. Palmini, L. Tassi, D. Schomer, F. Dubeau, F. Bartolomei, A. Yu, P. Krsek *et al.*, “Diagnostic utility of invasive eeg for epilepsy surgery: indications, modalities, and techniques,” *Epilepsia*, vol. 57, no. 11, pp. 1735–1747, 2016.
- [5] S. L. Moshé, E. Perucca, P. Ryvlin, and T. Tomson, “Epilepsy: new advances,” *The Lancet*, vol. 385, no. 9971, pp. 884–898, 2015.
- [6] S. Pequito, A. Ashourvan, D. Bassett, B. Litt, and G. J. Pappas, “Spectral control of cortical activity,” in *2017 American Control Conference (ACC)*, 2017.
- [7] A. Ashourvan, S. D. G. M. Pequito, A. N. Khambhati, F. Mikhail, and D. Bassett, “Model-based design for seizure control by stimulation,” *Journal of Neural Engineering*, vol. 17, no. 2, 2020.
- [8] S. Chang, X. Wei, F. Su, C. Liu, G. Yi, J. Wang, C. Han, and Y. Che, “Model predictive control for seizure suppression based on nonlinear auto-regressive moving-average volterra model,” *IEEE Transactions on Neural Systems and Rehabilitation Engineering*, vol. 28, no. 10, pp. 2173–2183, 2020.
- [9] S. Chatterjee, O. Romero, A. Ashourvan, and S. Pequito, “Fractional-order model predictive control as a framework for electrical neurostimulation in epilepsy,” *Journal of Neural Engineering*, vol. 17, no. 6, p. 066017, 2020.
- [10] K. Bieker, S. Peitz, S. L. Brunton, J. N. Kutz, and M. Dellnitz, “Deep model predictive flow control with limited sensor data and online learning,” *Theoretical and Computational Fluid Dynamics*, pp. 1–15, 2020.
- [11] N. Lanzetti, Y. Z. Lian, A. Cortinovis, L. Dominguez, M. Mercangöz, and C. Jones, “Recurrent neural network based mpc for process industries,” in *2019 18th European Control Conference (ECC)*. IEEE, 2019, pp. 1005–1010.
- [12] Andrzej, *Chaos, fractals, and noise : stochastic aspects of dynamics 1-2nd ed.* Springer-Verlag, 1994.
- [13] B. O. Koopman, “Hamiltonian systems and transformation in hilbert space,” *Proceedings of the national academy of sciences of the united states of america*, vol. 17, no. 5, p. 315, 1931.
- [14] J. Morton, F. D. Witherden, A. Jameson, and M. J. Kochenderfer, “Deep dynamical modeling and control of unsteady fluid flows,” in *Proceedings of the 32nd International Conference on Neural Information Processing Systems*, 2018, pp. 9278–9288.
- [15] N. Takeishi, Y. Kawahara, and T. Yairi, “Learning koopman invariant subspaces for dynamic mode decomposition,” in *Proceedings of the 31st International Conference on Neural Information Processing Systems*, 2017, pp. 1130–1140.
- [16] M. O. Williams, I. G. Kevrekidis, and C. W. Rowley, “A data-driven approximation of the koopman operator: Extending dynamic mode decomposition,” *Journal of Nonlinear Science*, vol. 25, no. 6, pp. 1307–1346, 2015.
- [17] M. Korda, M. Putinar, and I. Mezić, “Data-driven spectral analysis of the koopman operator,” *Applied and Computational Harmonic Analysis*, vol. 48, no. 2, pp. 599–629, 2020.
- [18] B. H. Jansen and V. G. Rit, “Electroencephalogram and visual evoked potential generation in a mathematical model of coupled cortical columns,” *Biological cybernetics*, vol. 73, no. 4, pp. 357–366, 1995.
- [19] C. D. Verdugo, S. Myren-Svelstad, E. Aydin, E. Van Hoeymissen, C. Deneubourg, S. Vanderhaeghe, J. Vancraeynest, R. Pelgrims, M. I. Cosacak, A. Muto *et al.*, “Glia-neuron interactions underlie state transitions to generalized seizures,” *Nature communications*, vol. 10, no. 1, pp. 1–13, 2019.
- [20] V. K. Jirsa, W. C. Stacey, P. P. Quilichini, A. I. Ivanov, and C. Bernard, “On the nature of seizure dynamics,” *Brain*, vol. 137, no. 8, pp. 2210–2230, 2014.
- [21] D. Fan and Q. Wang, “Closed-loop control of absence seizures inspired by feedback modulation of basal ganglia to the corticothalamic circuit,” *IEEE Transactions on Neural Systems and Rehabilitation Engineering*, vol. 28, no. 3, pp. 581–590, 2020.
- [22] A. van Rotterdam, F. L. Da Silva, J. Van den Ende, M. Viergever, and A. Hermans, “A model of the spatial-temporal characteristics of the alpha rhythm,” *Bulletin of mathematical biology*, vol. 44, no. 2, pp. 283–305, 1982.
- [23] K. Cho, B. Van Merriënboer, C. Gulcehre, D. Bahdanau, F. Bougares, H. Schwenk, and Y. Bengio, “Learning phrase representations using rnn encoder-decoder for statistical machine translation,” *arXiv preprint arXiv:1406.1078*, 2014.
- [24] T. Kajishima and K. Taira, “Computational fluid dynamics,” *Cham: Springer International Publishing*, no. 1, 2017.
- [25] A. L. Hodgkin and A. F. Huxley, “A quantitative description of membrane current and its application to conduction and excitation in nerve,” *The Journal of physiology*, vol. 117, no. 4, pp. 500–544, 1952.
- [26] B. Lusch, J. N. Kutz, and S. L. Brunton, “Deep learning for universal linear embeddings of nonlinear dynamics,” *Nature communications*, vol. 9, no. 1, pp. 1–10, 2018.

APPENDIX

A. EEG synthesis with Jansen-Rit Model

The Jansen-Rit model was originally proposed by Jansen and Rit in 1995 for studying the cortical column [18]. It is a neural population model of a local cortical circuit. In particular, the model consists of three subpopulations, the pyramidal neurons, the excitatory feedback interneurons and the inhibitory feedback interneurons. The dynamics between these three neuronal populations reflect the feedback loop in a single cortical area of the human brain [18]. Dynamics in larger brain area could be modelled by a multiple area model composed of multiple neural masses.

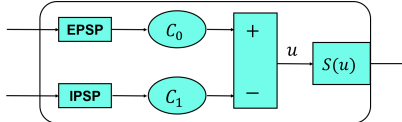


Fig. 5. An outline for the neural mass model. External stimuli are converted to the postsynaptic potentials via the PSP transform. These potentials are then scaled by some constants C representing the average number of synapses receiving the stimuli. After summing up all excitatory potentials and subtracting all inhibitory potentials, we obtain the average membrane potential u . Finally, a sigmoid function is used to transform the u to average pulse rate.

As shown in Figure 5, a neural mass model has two main quantities, the average pulse densities and the average membrane potential. The average pulse densities typically result from external stimuli and stimuli produced by other neural masses. Each input to the neural mass will be converted from an average pulse density to a potential via a Post Synaptic Potential function (PSP). In particular, excitatory post synaptic potential (EPSP) function is specifically designed for the conversion of input pulses from the excitatory interneurons, while inhibitory synaptic potential (IPSP) function is designed for the conversion of input pulses from the inhibitory interneurons. Each of these potentials is then scaled by a certain constant C representing the average number of synapses connected to this neural mass population. After that, the average membrane potential u will be computed by summing up all the potentials from the excitatory interneurons and subtracting the inhibitory counterparts. At the end of this process, the average membrane potential u will be converted to average pulse density again by the potential-to-rate function S and sent to other neurons. This represents the firing phenomena of this neural mass population.

In the Jansen-Rit model, the PSP function is given by the solution of the second order differential equation,

$$\begin{cases} \frac{dx}{dt} = y \\ \frac{dy}{dt} = Qqz - 2qy - q^2x. \end{cases} \quad (13)$$

Here the input variable $z(t)$ represents the average pulse density (or firing rate) and $x(t)$ is the output of the PSP function. Fortunately, the solutions of this set of ordinary differential equation have closed analytic form and are referred to as the excitatory transfer function $h_e(t) = Aae^{-at}$ and the inhibitory transfer function $h_i(t) = Bbe^{-bt}$. Here

the amplitudes A and B denote the average synaptic gains, while the phase coefficients a and b represents the average time constants. The potential-to-rate function converts the average membrane potential to the average pulse density, and is usually taken to be a non-decreasing function converged to zero as $u \rightarrow -\infty$ and bounded from above. A common choice is the Sigmoid function $S(v) = \frac{2e_0}{1+e^{r(v_0-v)}}$ where $2e_0$ represents the maximum firing rate, v_0 is the post-synaptic potential equal to half maximum firing rate, and r is the steepness of the sigmoid function. Combining the above components, the Jansen-Rit model is given by the following dynamical system (for single cortical column),

1) Single Cortical Column Jansen Rit Model:

$$\begin{cases} \dot{y}_1 = y_4 \\ \dot{y}_4 = AaS(y_2 - y_3) - 2ay_4 - a^2y_1 \\ \dot{y}_2 = y_5 + d(t) \\ \dot{y}_5 = Aa(p + C_2S(C_1y_1)) - 2ay_5 - a^2y_2 \\ \dot{y}_3 = y_6 \\ \dot{y}_6 = BbC_4S(C_3y_1) - 2by_6 - b^2y_3 \end{cases} \quad (14)$$

The parameters for the single cortical column Jansen-Rit Model are provided in the table below. These values were originally set by Van Rotterdam et al. [22].

2) Double column Jansen-Rit: As shown in Figure 6, the cortical column was connected with corresponding connectivity constants. For each column, it is fed by two inputs: an external one, which can be different for each column, and another one coming from the output of other column. A delay parameter a_d was introduced for measuring the delay of signal transfer.

$$\begin{cases} \dot{y}_0 = y_3 \\ \dot{y}_3 = AaS(y_1 - y_2) - 2ay_3 - a^2y_0 \\ \dot{y}_1 = y_4 \\ \dot{y}_4 = Aa(p + C_2S(C_1y_0) + K_2y_{13}) - 2ay_4 - a^2y_1 \\ \dot{y}_2 = y_5 \\ \dot{y}_5 = BbC_4S(C_3y_0) - 2by_5 - b^2y_2 \\ \dot{y}_6 = y_9 \\ \dot{y}_9 = A'aS(y_7 - y_8) - 2ay_9 - a^2y_6 \\ \dot{y}_7 = y_{10} \\ \dot{y}_{10} = A'a(p' + C'_2S(C'_1y_6) + K_1y_{12}) - 2ay_{10} - a^2y_7 \\ \dot{y}_8 = y_{11} \\ \dot{y}_{11} = B'bC'_4S(C'_3y_6) - 2by_{11} - b^2y_8(t) \\ \dot{y}_{12} = y_{14} \\ \dot{y}_{14} = A'a_dS(y_1 - y_2) - 2a_dy_{14} - a^2y_{12} \\ \dot{y}_{13} = y_{15} \\ \dot{y}_{15} = A'a_dS(y_7 - y_8) - 2a_dy_{15} - a^2y_{13} \end{cases} \quad (15)$$

The experiment parameters for the double cortical column Jansen-Rit Model are provided in the table below. We can change them according to the target column we preferred.

B. System Identification

1) Koopman-operator based autoencoder: The deep Koopman-operator based autoencoder consists of an encoder, a linear transformation layer, and a decoder. The parameters are summarized in the following table.

TABLE II

PARAMETERS FOR SINGLE CORTICAL COLUMN JANSEN-RIT MODEL

Parameters	Description	Values
A	Average excitatory synaptic gain	7.8 mV
B	Average inhibitory synaptic gain	22 mV
a	Reciprocal of excitatory time constant	100 Hz
b	Reciprocal of inhibitory time constant	50 Hz
v_0	Potential at half of the maximum firing rate of Sigmoid function	6 mV
r	Steepness of Sigmoid function	0.56 mV
e_0	Half of the maximum firing rate of Sigmoid function	2.5 Hz
C_1	Average synaptic connectivity	135
C_2	Average synaptic connectivity	108
C_3	Average synaptic connectivity	33.75
C_4	Average synaptic connectivity	33.75

TABLE III

PARAMETERS FOR DOUBLE CORTICAL COLUMNS JANSEN-RIT MODEL

Parameters	Description	Values
A	Average excitatory synaptic gain	7.8 mV
B	Average inhibitory synaptic gain	22 mV
C_1	Average synaptic connectivity	135
C_2	Average synaptic connectivity	108
C_3	Average synaptic connectivity	33.75
C_4	Average synaptic connectivity	33.75
A'	Average excitatory synaptic gain	7 mV
B'	Average inhibitory synaptic gain	22 mV
C'_1	Average synaptic connectivity	135
C'_2	Average synaptic connectivity	108
C'_3	Average synaptic connectivity	33.75
C'_4	Average synaptic connectivity	33.75
a_d	Reciprocal of excitatory time constant with latency	$a/3$
a	Reciprocal of excitatory time constant	100 Hz
b	Reciprocal of inhibitory time constant	50 Hz
v_0	Potential at half of the maximum firing rate of Sigmoid function	6 mV
r	Steepness of Sigmoid function	0.56 mV
e_0	Half of the maximum firing rate of Sigmoid function	2.5 Hz
K_1	Connectivity constants	100
K_2	Connectivity constants	100

TABLE IV

PARAMETERS FOR KOOPMAN-OPERATOR BASED AUTOENCODER

Parameters	Description	Values
T	Time length of the input metrics	60
H_1	Units of hidden layer in the encoder network	60
H_2	Units of hidden layer in the decoder network	60
L_R	Learning rate	0.001
F	Data sampling rate	50 HZ
T_p	Time length of the prediction	20

2) Recurrent Neural Network for System Identification:

An RNN-based model models a discrete-time dynamical process with a sequence of multi-step ahead predictions in a concatenating form, as shown in Figure 7. We employed a Gated Recurrent Unit (GRU), a variant of Long Short-Term Memory (LSTM), as the RNN structure [23]. An additional dense layer was trained for capturing the mapping relationship between the previous input/output signals and the initial states of GRU. Also, another dense layer was trained for mapping the GRU states to output signals.

The RNN can be summarized as a unified discrete-time dynamical form:

$$\begin{aligned} x_{k+1} &= f(x_k, u_k) \\ y_{k+1} &= h(x_{k+1}) \end{aligned} \quad (16)$$

where $u_k \in \mathbb{R}^m$, $y_k \in \mathbb{R}^n$, and $x_k \in \mathbb{R}^p$, m is the input dimension, n is the output dimension while p is the number of hidden states.

As an identification model in the MPC built-in process, the GRU can be written in the following explicit expression,

$$\begin{aligned} z_k &= \text{hard_sigmoid}(W_i^z v_k + W_x^z x_k + b^z) \\ r_k &= \text{hard_sigmoid}(W_i^r v_k + W_x^r x_k + b^r) \\ h_k &= \tanh(W_i^h v_k + W_x^h (r_k \circ x_k) + b^h) \\ x_{k+1} &= z_k \circ x_k + (1 - z_k) \circ h_k \end{aligned} \quad (17)$$

where $W_i^z, W_x^z, W_i^r, W_x^r$ represent the input weights,

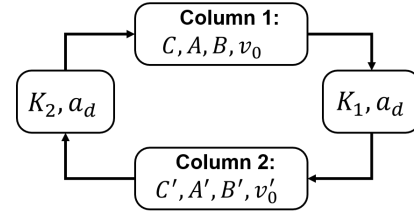


Fig. 6. The design of two interactive cortical columns

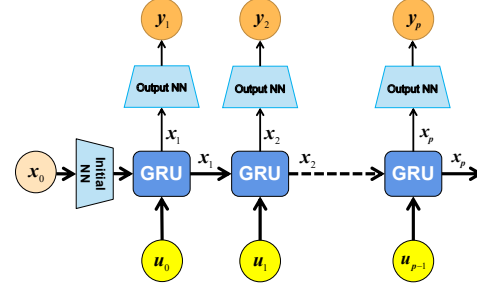


Fig. 7. The network structure of RNN: A GRU based RNN Model

W_x^z, W_x^r, W_x^h represent the recurrent weights and b^z, b^r, b^h denote bias in the corresponding gates. The symbol \circ denotes element-wise multiplication.

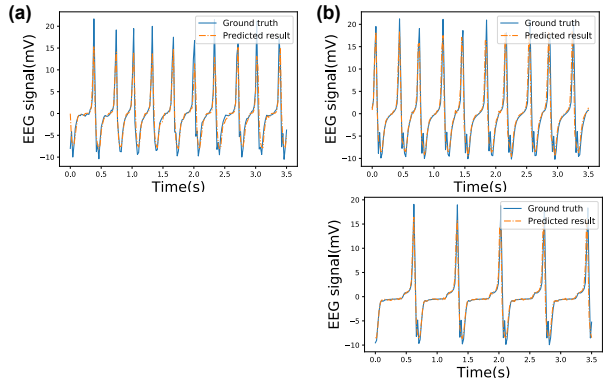


Fig. 8. GRU Predictive Performance

GRU serves as a predictive model (identified model) for modelling the unknown black-box seizure-wave dynamics. The structure of our RNN model has high scalability for modeling the input-output data into a low/high-dimensional latent space. Fig. 8 shows the predictive result in both single (Fig. 8(a)) or double cortical columns (Fig. 8(b)).

TABLE V
PARAMETER VALUES FOR THE GRU MODEL

Parameters	Description	Values
M	Number of previous inputs	24
N	Number of previous outputs	25
T_p	Prediction length	175
F	Data sampling rate	50 HZ
B	Batch size	30
U_1	Units of hidden layer in initial neural network	60
U_2	Units of hidden layer in output neural network	60
U_3	Units of GRU cells in one column prediction	60
U_4	Units of GRU cells in two column prediction	60